

Extended Fourier analysis of signals

Abstract. The extended summary of Dr.Sc.Comp. thesis [6] is created to emphasize the tight connection of the proposed spectral analysis method with the Discrete Fourier Transform (DFT) - the most extensively studied and frequently used approach in the history of signal processing. It is shown that in a typical application case, where uniform data readings are transformed to the same number of uniformly spaced frequencies, the results of the classical DFT and proposed approach coincide. The difference in performance appears when the length of the DFT is selected greater than the length of the data. The DFT solves the unknown data problem by padding readings with zeros up to the length of the DFT, while the proposed Extended DFT (EDFT) deals with this situation in a different way, it uses the Fourier integral transform as a target and optimizes the transform basis in the extended frequency range without putting such restrictions on the time domain. Thus, the Inverse DFT (IDFT) applied to the result of EDFT returns not only known readings but also the extrapolated data, where classical DFT is able to give back just zeros. The EDFT significantly extends the usability of the DFT based methods, where previously these approaches were considered inapplicable [8-32]. The EDFT finds the solution in an iterative way and requires repeated calculations to get the adaptive basis, and this makes its numerical complexity much higher compared to DFT. This disadvantage was a serious problem in 1990s, when the method has been proposed. Fortunately, since then the power of computers has increased so much that nowadays EDFT application could be considered as a real alternative.

Table of Contents

Extended Fourier analysis of signals.....	1
1 Introduction.....	2
2 Problem formulation.....	2
2.1 Basic expressions of classical Fourier analysis.....	2
2.2 Basic expressions of extended Fourier analysis.....	3
3 Problem solution.....	5
3.1 Extended Fourier transform of continuous time signals.....	5
3.2 Extended Discrete Time Fourier Transform.....	6
3.2.1 A particular solution for discrete time signals.....	6
3.2.2 Generalized solution for discrete time signals.....	7
3.3.3 Iterative EDTFT algorithm.....	8
4 Extended DFT algorithm.....	8
5 EDFT and other nonparametric approaches.....	10
5.1 Capon filter approach.....	10
5.2 GWLS solution.....	12
5.3 High-Resolution DFT.....	12
6 Computer simulations.....	13
7 EDFT algorithm in MATLAB code.....	20
8 References.....	20

1 Introduction

A Fourier transform is a powerful tool of signal analysis and representation of a real or complex-valued function of time $x(t)$ (hereinafter referred to as the signal) in the frequency domain

$$F(\omega) = \int_{-\infty}^{\infty} x(t) e^{-j\omega t} dt, \quad (1.1)$$

$$x(t) = \frac{1}{2\pi} \int_{-\infty}^{\infty} F(\omega) e^{j\omega t} d\omega. \quad (1.2)$$

The Fourier transforms orthogonality property

$$\int_{-\infty}^{\infty} e^{j\omega_1 t} e^{-j\omega_2 t} dt = 2\pi \delta(\omega_1 - \omega_2) \quad (2)$$

providing a basis for the signal selective frequency analysis, where ω, ω_0 are cyclic frequencies and $\delta(\omega - \omega_0)$ is the Dirac delta function. Unfortunately, the Fourier transforms calculation according to (1.1) requiring knowledge of the signal $x(t)$ as well as performing of integration operation in infinite time interval. Therefore, for practical evaluation of (1.1) numerically, the signal observation period and the interval of integration is always limited by some finite value Θ , $-\Theta/2 \leq t \leq \Theta/2$. The same applies to the Fourier analysis of the signal $x(t)$ sampled versions: nonuniformly sampled signal $x(t_k)$ or uniformly sampled signal $x(kT)$, $k = -\infty, \dots, -1, 0, 1, \dots, +\infty$. Only a finite length sequence $x(t_k)$ or $x(kT)$, $k = 0, 1, 2, \dots, K-1$, are subject of Fourier analysis, where K is a discrete sequence length, T is sampling period and the signal observation period $\Theta = t_{K-1} - t_0$ or $\Theta = KT$. To avoid aliasing and satisfy the Nyquist limit, uniform sampling of continuous time signal should be performed with the sampling period $T \leq \pi/\Omega$, where Ω is upper cyclic frequency of signal $x(t)$. Although nonuniform sampling has no such strict limitation on the mean sampling period $T_s = \Theta/K$, the following analysis we suppose that both sequences, $x(t_k)$ and $x(kT)$, are derived from the band-limited in Ω signal $x(t)$. Let write the basic expressions of the classical and the proposed extended Fourier analysis of continuous time signal $x(t)$ and its sampled versions $x(t_k)$ and $x(kT)$.

2 Problem formulation

“The formulation of a problem is often more essential than its solution which may be merely a matter of mathematical or experimental skill.”

Albert Einstein

2.1 Basic expressions of classical Fourier analysis

The classical Fourier analysis dealing with the following finite time Fourier transforms

$$F_{\Theta}(\omega) = \int_{-\Theta/2}^{\Theta/2} x(t) e^{-j\omega t} dt, \quad (3.1a)$$

$$F_{\Theta}(\omega) = \sum_{k=0}^{K-1} x(t_k) e^{-j\omega t_k}, \quad (3.1b)$$

$$F_{\Theta}(\omega) = \sum_{k=0}^{K-1} x(kT) e^{-j\omega kT}, \quad (3.1c)$$

$$x_{\Theta}(t) = \frac{1}{2\pi} \int_{-\Omega}^{\Omega} F_{\Theta}(\omega) e^{j\omega t} d\omega. \quad (3.2)$$

where (3.2) is the inverse Fourier transform obtained from (1.2) for band-limited in Ω signal. Transforms (3.1b) and (3.1c) are known as Discrete Time Fourier Transforms (DTFT) of

nonuniformly and uniformly sampled signals. The values of reconstructed signal $x_{\Theta}(t)$ outside the observation period Θ are zeros or vanishes depending on whether (3.2) applies to the results (3.1a) or (3.1b) and (3.1c).

The signal amplitude spectrum is the Fourier transform (3.1) divided by the observation period Θ ,

$$S_{\Theta}(\omega) = \frac{1}{\Theta} F_{\Theta}(\omega). \quad (4)$$

The frequency resolution of the classical Fourier analysis is inversely proportional to the signal observation period Θ .

Obviously, one can get the formula (3.1a) by truncation of infinite integration limits in (1.1) and the DTFT (3.1a) and (3.1b) as result of replacement of infinite sums by finite ones. This mean, the classical Fourier analysis supposed that the signal outside Θ is zeros. In other words, the Fourier transform calculation by formulas (3.1) is well justified if applied to time-limited within Θ signals. On the other hand, a band-limited in Ω signal cannot be also time-limited and obviously have nonzero values outside Θ . Generally, the Fourier analysis results obtained by using the exponential basis tend to the Fourier transform, if $\Theta \rightarrow \infty$, while in any finite Θ there may exist another transform basis providing a more accurate estimation of (1.1).

2.2 Basic expressions of extended Fourier analysis

The idea of extended Fourier analysis is finding the transform basis, applicable for a band-limited signals registered in finite time interval Θ and providing the results as close as possible to the Fourier transform (1.1) defined in infinite time interval. The formulas for proposed extended Fourier analysis could be written as

$$F_{\alpha}(\omega) = \int_{-\Theta/2}^{\Theta/2} x(t)\alpha(\omega, t)dt, \quad (5.1a)$$

$$F_{\alpha}(\omega) = \sum_{k=0}^{K-1} x(t_k)\alpha(\omega, t_k), \quad (5.1b)$$

$$F_{\alpha}(\omega) = \sum_{k=0}^{K-1} x(kT)\alpha(\omega, kT), \quad (5.1c)$$

$$x_{\alpha}(t) = \frac{1}{2\pi} \int_{-\Omega}^{\Omega} F_{\alpha}(\omega)e^{j\omega t} d\omega, \quad (5.2)$$

where in general case the transform basis $\alpha(\omega, t)$, $\alpha(\omega, t_k)$ and $\alpha(\omega, kT)$ are not equal to the classical ones (3.1). Note that the inverse Fourier transform (5.2) still holds the exponential basis. To ensure that the results of transforms (5.1) are close to the result of the Fourier transform (1.1) for the signal $x(t)$, the following minimum least squares expression will be composed and solved

$$|F(\omega) - F_{\alpha}(\omega)|^2 \rightarrow \min. \quad (6)$$

Unfortunately, as already stated above, the calculation of $F(\omega)$ for a band-limited signal cannot be performed directly. So, in order to compose (6), we should find an adequate substitution. Let's recall that a complex exponent, at cyclic frequency ω_0 and with a complex amplitude $S(\omega_0)$, is defined in infinite time interval as

$$x(\omega_0, t) = S(\omega_0)e^{j\omega_0 t}, -\infty < t < \infty. \quad (7)$$

The Fourier transform of a signal (7) can be expressed by the Dirac delta function (2)

$$\int_{-\infty}^{\infty} x(\omega_0, t)e^{-j\omega t} dt = 2\pi S(\omega_0)\delta(\omega - \omega_0). \quad (8)$$

Now, let's use (7) as a signal model with known amplitude spectrum $S(\omega_0)$ for frequencies in range $-\Omega \leq \omega_0 \leq \Omega$ and, in the minimum least square expression (6), substitute $F(\omega)$ by the signal model Fourier transform (8) and the signals $x(t)$, $x(t_k)$ and $x(kT)$ in (5.1) by the signal models (7), correspondingly. Finally, the integral least square error estimators for all the three signal cases get the following form

$$\Delta = \int_{-\Omega}^{\Omega} \left| 2\pi S(\omega_0) \delta(\omega - \omega_0) - \int_{-\Theta/2}^{\Theta/2} S(\omega_0) e^{j\omega_0 t} \alpha(\omega, t) dt \right|^2 d\omega_0, \quad (9a)$$

$$\Delta = \int_{-\Omega}^{\Omega} \left| 2\pi S(\omega_0) \delta(\omega - \omega_0) - \sum_{k=0}^{K-1} S(\omega_0) e^{j\omega_0 t_k} \alpha(\omega, t_k) \right|^2 d\omega_0, \quad (9b)$$

$$\Delta = \int_{-\Omega}^{\Omega} \left| 2\pi S(\omega_0) \delta(\omega - \omega_0) - \sum_{k=0}^{K-1} S(\omega_0) e^{j\omega_0 kT} \alpha(\omega, kT) \right|^2 d\omega_0. \quad (9c)$$

The solutions of (9) for a definite signal model (7) provide the basis $\alpha(\omega, t)$, $\alpha(\omega, t_k)$ and $\alpha(\omega, kT)$ for the extended Fourier transforms (5.1). To control how close the selected signal model amplitudes $S(\omega_0)$ are to the signals $x(t)$, $x(t_k)$ and $x(kT)$ amplitude spectrum, we will find the formulas for estimate signal amplitude spectrum $S_\alpha(\omega)$ in the extended Fourier basis $\alpha(\omega, t)$, $\alpha(\omega, t_k)$ and $\alpha(\omega, kT)$.

The formula (8) is showing the connection between the signal model Fourier transform and its amplitude spectrum, from where $S(\omega_0)$ could be expressed as signal model Fourier transform divided by $2\pi\delta(\omega - \omega_0)$. Taking (8) into account, $S_\alpha(\omega)$ is calculated as the transforms (5.1) divided by the estimate of $2\pi\delta(\omega - \omega_0)$ in the extended Fourier basis, which is determined from (9) in the case $\Delta=0$ and $\omega_0=\omega$,

$$S_\alpha(\omega) = \frac{\int_{-\Theta/2}^{\Theta/2} x(t) \alpha(\omega, t) dt}{\int_{-\Theta/2}^{\Theta/2} e^{j\omega t} \alpha(\omega, t) dt}, \quad (10a)$$

$$S_\alpha(\omega) = \frac{\sum_{k=0}^{K-1} x(t_k) \alpha(\omega, t_k)}{\sum_{k=0}^{K-1} e^{j\omega t_k} \alpha(\omega, t_k)}, \quad (10b)$$

$$S_\alpha(\omega) = \frac{\sum_{k=0}^{K-1} x(kT) \alpha(\omega, kT)}{\sum_{k=0}^{K-1} e^{j\omega kT} \alpha(\omega, kT)}, \quad (10c)$$

and showing that the amplitude spectrum on the frequency ω is estimated as ratio of the signal extended Fourier transform to the transform of exponent with a unit amplitude in the same basis. This is true also for classical Fourier transform. For example, after substituting exponential basis $\alpha(\omega, t) = e^{-j\omega t}$ in (10a), the denominator becomes equal to Θ as in formula (4) for the classical Fourier analysis.

Values of the denominator in formulas (10) are in inverse ratio to the frequency resolution of the extended Fourier transform.

Before finding the the extended basis functions for arbitrary $S(\omega_0)$, it is reasonable to consider a simple signal model having a rectangular form, $S(\omega_0)=1$ for $-\Omega \leq \omega_0 \leq \Omega$ and zeros outside. Then the estimators (9) reduces to

$$\Delta = \int_{-\Omega}^{\Omega} \left| 2\pi\delta(\omega - \omega_0) - \int_{-\Theta/2}^{\Theta/2} e^{j\omega_0 t} \alpha(\omega, t) dt \right|^2 d\omega_0, \quad (11a)$$

$$\Delta = \int_{-\Omega}^{\Omega} \left| 2\pi\delta(\omega - \omega_0) - \sum_{k=0}^{K-1} e^{j\omega_0 t_k} \alpha(\omega, t_k) \right|^2 d\omega_0, \quad (11b)$$

$$\Delta = \int_{-\Omega}^{\Omega} \left| 2\pi\delta(\omega - \omega_0) - \sum_{k=0}^{K-1} e^{j\omega_0 kT} \alpha(\omega, kT) \right|^2 d\omega_0. \quad (11c)$$

The solution of (11) allows to establish relationship between the classical and extended Fourier analysis.

3 Problem solution

In this section the integral least square error estimators (9) and (11) are solved and subsequent analysis of the obtained results are performed to find out the only those solutions that can lead to practically realizable algorithms.

3.1 Extended Fourier transform of continuous time signals

The solution of (11a) for continuous time signal $x(t)$ is found as a partial derivation $\frac{\partial \Delta}{\partial \alpha(\omega, \tau)} = 0$, $-\Theta/2 \leq \tau \leq \Theta/2$, and leads to the linear integral equation

$$\int_{-\Theta/2}^{\Theta/2} \frac{\sin(\Omega(t-\tau))}{\pi(t-\tau)} \alpha(\omega, t) dt = e^{-j\omega\tau}. \quad (12)$$

Step by step solution of (12) is given in [2]. Finally, the basis $\alpha(\omega, t)$ are obtained by applying a specific functions system - a prolate spheroidal wave functions $\psi_k(t)$, $k=0,1,2,\dots$ and are written as series expansion

$$\alpha(\omega, t) = \sum_{k=0}^{\infty} \frac{B_k(\omega)}{\lambda_k} \psi_k(t). \quad (13)$$

The extended Fourier Transform of continuous time signal $x(t)$ are given by

$$F_{\alpha}(\omega) = \sum_{k=0}^{\infty} B_k(\omega) a_k, \quad -\Omega \leq \omega \leq \Omega, \quad (14.1)$$

$$x_{\alpha}(t) = \sum_{k=0}^{\infty} \psi_k(t) a_k, \quad -\infty < t < \infty, \quad (14.2)$$

$$S_{\alpha}(\omega) = \frac{\sum_{k=0}^{\infty} B_k(\omega) a_k}{\sum_{k=0}^{\infty} |B_k(\omega)|^2}, \quad (14.3)$$

where $a_k = \frac{1}{\lambda_k} \int_{-\Theta/2}^{\Theta/2} x(\tau) \psi_k(\tau) d\tau$, $\lambda_k = \int_{-\Theta/2}^{\Theta/2} \psi_k^2(t) dt$ and $B_k(\omega) = \sqrt{\frac{\pi\Theta}{\lambda_k \Omega}} \psi_k\left(\omega \frac{\Theta}{2\Omega}\right) (-j)^k$.

The extended Fourier transform in accordance with (14.1) requesting a calculations of infinite sums, this mean, an infinite quantity of mathematical operations, therefore it's impossible for real world applications. Theoretically, the value of denominator $\sum_{k=0}^K |B_k(\omega)|^2$ in amplitude spectrum

formula (14.3) tends to infinite for $K \rightarrow \infty$, and the extended Fourier transform (14.1) provide a super-resolution - an ability to determine the Fourier transform for the sum of sinusoids or

complex exponents, if frequencies of them differ by arbitrary small finite value.

3.2 Extended Discrete Time Fourier Transform

In this subsection the minimum least square error estimators (9b,c) and (11b,c) are solved and the extended Fourier transforms for uniformly and nonuniformly sampled complex-valued signals are obtained. The proposed approaches have been developed in articles [3] and [4], where the derivations for real-valued discrete signals are given.

Please note that the following notations are used in the matrix equations:

- superscripts $\mathbf{X}^{-1}, \mathbf{X}^T, \mathbf{X}^*, \mathbf{X}^H$ denote inverse, transpose, complex conjugate, Hermitian (complex conjugate) transpose of the matrix \mathbf{X} ;
- $/$ represents element-by-element division of two matrices with the same size;
- $sum(\mathbf{X})$ means addition of all matrix \mathbf{X} elements;
- $diag(\mathbf{X})$ forms the row vector by extracting the main diagonal elements from quadratic matrix \mathbf{X} or it puts the elements of vector \mathbf{X} on the main diagonal to form a diagonal matrix.

3.2.1 A particular solution for discrete time signals

The solutions of (11b,c) can be obtained similarly to (11a) as partial derivatives of $\frac{\partial \Delta}{\partial \alpha(\omega, t_l)} = 0$ and $\frac{\partial \Delta}{\partial \alpha(\omega, lT)} = 0$, $l=0,1,2,\dots,K-1$, and leads to the systems of linear equations

$$\sum_{k=0}^{K-1} \frac{\sin(\Omega(t_k - t_l))}{\pi(t_k - t_l)} \alpha(\omega, t_k) = e^{-j\omega t_l}, \quad (15.1)$$

$$\sum_{k=0}^{K-1} \frac{\sin(\Omega(k-l)T)}{\pi(k-l)T} \alpha(\omega, kT) = e^{-j\omega lT}. \quad (15.2)$$

The solution of (15) in the matrix form is expressed as

$$\mathbf{A}_\omega = \mathbf{R}^{-1} \mathbf{E}_\omega, \quad (16)$$

where $\mathbf{A}_\omega (K \times 1)$ and $\mathbf{E}_\omega (K \times 1)$ are the extended Fourier and the exponential basis.

The formulas of Extended Discrete Time Fourier Transform (EDTFT) for signal model $S(\omega_0)=1$, $-\Omega \leq \omega_0 \leq \Omega$, are derived by substituting of transform basis (16) into expressions (5) and (10)

$$F_\alpha(\omega) = \mathbf{x} \mathbf{R}^{-1} \mathbf{E}_\omega, \quad -\Omega \leq \omega \leq \Omega, \quad (17.1)$$

$$x_\alpha(t) = \mathbf{x} \mathbf{R}^{-1} \mathbf{E}_t, \quad -\infty < t < \infty, \quad (17.2)$$

$$S_\alpha(\omega) = \frac{\mathbf{x} \mathbf{R}^{-1} \mathbf{E}_\omega}{\mathbf{E}_\omega^H \mathbf{R}^{-1} \mathbf{E}_\omega}. \quad (17.3)$$

The matrices for nonuniformly sampled signal case are composed as follows

$$\mathbf{x} (1 \times K) - x(t_k), \mathbf{E}_\omega (K \times 1) - e^{-j\omega t_l}, \mathbf{R} (K \times K) - r_{l,k} = \frac{\sin \Omega(t_k - t_l)}{\pi(t_k - t_l)} \text{ and } \mathbf{E}_t (K \times 1) - \frac{\sin \Omega(t - t_l)}{\pi(t - t_l)}.$$

Uniformly sampled sequence $x(kT)$ can be considered as a special case of nonuniform sampling at time moments $t_k=kT$, $k=0,1,2,\dots,K-1$. Then the matrices elements in (16, 17) are

$$\mathbf{x} (1 \times K) - x(kT), \mathbf{E}_\omega (K \times 1) - e^{-j\omega lT}, \mathbf{R} (K \times K) - r_{l,k} = \frac{\sin \Omega(k-l)T}{\pi(k-l)T}, \mathbf{E}_t (K \times 1) - \frac{\sin \Omega(t-lT)}{\pi(t-lT)}.$$

In particular, if sampling of signal $x(kT)$ is done with Nyquist rate, $T=\pi/\Omega$, the matrix \mathbf{R} becomes a unit matrix \mathbf{I} and the formula (17.1) coincide with classical DTFT (3.1c), but the formula (17.3) reduces to well known relationship between discrete signal Fourier transform and

its amplitude spectrum

$$F_\alpha(\omega) = F_\Theta(\omega) = \mathbf{x}\mathbf{E}_\omega, \quad (18.1)$$

$$S_\alpha(\omega) = \frac{1}{K} \mathbf{x}\mathbf{E}_\omega. \quad (18.2)$$

Whereas for nonuniformly sampled signal $x(t_k)$ the matrix $\mathbf{R} \neq \mathbf{I}$, even if mean sampling period $T_s = \pi/\Omega$ and formulas (17) give results superior to those that obtained by the classical nonuniform DTFT (3.1b). For oversampled signals, T (or T_s) $< \pi/\Omega$, the EDTFT approach can provide a high frequency resolution and improved spectral estimation quality. Unfortunately an achievement of such results is limited by finite precision in the mathematical calculations and by restrictions on frequency range in the process of signal sampling. Theoretical value of denominator in (17.3) $\mathbf{E}_\omega^H \mathbf{R}^{-1} \mathbf{E}_\omega = K$ and the frequency resolution should increase proportionally to the number of samples in the signal observation period Θ . In the border-case, if number of samples within Θ increasing infinitely, $K \rightarrow \infty$, and the discrete time signal tends to the continuous time signal $x(t)$, the EDTFT (17.1) gives the same results as (14.1).

3.2.2 Generalized solution for discrete time signals

Now, let consider the solution of the minimum least square error estimators (9b,c) for arbitrary selected signal model $S(\omega_0)$. The derivation formulas for both estimators are similar to ones given in previous section. For example, a partial derivation of (9b) by basis functions

$\frac{\partial \Delta}{\partial \alpha(\omega, t_l)} = 0$, for $l = 0, 1, 2, \dots, K-1$, provide the least square solution

$$\int_{-\Omega}^{\Omega} \left(2\pi S(\omega_0) \delta(\omega - \omega_0) - \sum_{k=0}^{K-1} S(\omega_0) e^{j\omega_0 t_k} \alpha(\omega, t_k) \right) S^*(\omega_0) e^{-j\omega_0 t_l} d\omega_0 = 0, \quad (19)$$

Equation (19) can be rewritten as

$$\sum_{k=0}^{K-1} \left(\int_{-\Omega}^{\Omega} |S(\omega_0)|^2 e^{j\omega_0(t_k - t_l)} d\omega_0 \right) \alpha(\omega, t_k) = 2\pi \int_{-\Omega}^{\Omega} |S(\omega_0)|^2 e^{-j\omega_0 t_l} \delta(\omega - \omega_0) d\omega_0. \quad (20)$$

The filtering feature of Dirac delta function $\int_{-\infty}^{\infty} f(x) \delta(x - x_0) dx = f(x_0)$ applied to the right part of (20) gives the final form of the system of linear equations

$$\sum_{k=0}^{K-1} \left(\frac{1}{2\pi} \int_{-\Omega}^{\Omega} |S(\omega_0)|^2 e^{j\omega_0(t_k - t_l)} d\omega_0 \right) \alpha(\omega, t_k) = |S(\omega)|^2 e^{-j\omega t_l}, \quad (21.1)$$

$$\sum_{k=0}^{K-1} \left(\frac{1}{2\pi} \int_{-\Omega}^{\Omega} |S(\omega_0)|^2 e^{j\omega_0(k-l)T} d\omega_0 \right) \alpha(\omega, kT) = |S(\omega)|^2 e^{-j\omega lT}, \quad (21.2)$$

for $l=0, 1, 2, \dots, K-1$, where $|S(\omega)|^2$ is the signal model power at $\omega_0 = \omega$. The equations (21.2) are applicable for uniformly sampled signal $x(kT)$ and can be derived from (9c) in a similar way as (21.1). The EDTFT basis \mathbf{A}_ω ($K \times 1$) - $\alpha(\omega, t_k)$ or $\alpha(\omega, kT)$ are found as a solution of (21)

$$\mathbf{A}_\omega = |S(\omega)|^2 \mathbf{R}^{-1} \mathbf{E}_\omega. \quad (22)$$

Substituting of transform basis (22) into expressions (5) and (10), yields the formulas for calculation of the EDTFT:

$$F_\alpha(\omega) = \mathbf{x}\mathbf{A}_\omega = |S(\omega)|^2 \mathbf{x}\mathbf{R}^{-1} \mathbf{E}_\omega, \quad -\Omega \leq \omega \leq \Omega, \quad (23.1)$$

$$x_\alpha(t) = \mathbf{x}\mathbf{R}^{-1} \mathbf{E}_t, \quad -\infty < t < \infty, \quad (23.2)$$

$$S_\alpha(\omega) = \frac{\mathbf{x}\mathbf{A}_\omega}{\mathbf{E}_\omega^H\mathbf{A}_\omega} = \frac{\mathbf{x}|S(\omega)|^2\mathbf{R}^{-1}\mathbf{E}_\omega}{\mathbf{E}_\omega^H|S(\omega)|^2\mathbf{R}^{-1}\mathbf{E}_\omega} = \frac{\mathbf{x}\mathbf{R}^{-1}\mathbf{E}_\omega}{\mathbf{E}_\omega^H\mathbf{R}^{-1}\mathbf{E}_\omega} \quad (23.3)$$

The elements of matrix \mathbf{R} ($K \times K$) in the formulas (22, 23) are expressed by integrals

$$r_{l,k} = \frac{1}{2\pi} \int_{-\Omega}^{\Omega} |S(\omega_0)|^2 e^{j\omega_0(t_k - t_l)} d\omega_0, \quad (24.1)$$

$$r_{l,k} = \frac{1}{2\pi} \int_{-\Omega}^{\Omega} |S(\omega_0)|^2 e^{j\omega_0(k-l)T} d\omega_0, \quad (24.2)$$

for nonuniformly and uniformly sampled signal \mathbf{x} ($1 \times K$) cases, correspondingly. If the signal and its model power spectra are close, $|S_\alpha(\omega)|^2 \approx |S(\omega)|^2$, then the matrix \mathbf{R} elements (24) are also an estimate of the autocorrelation function for the sequence \mathbf{x} . Similarly, the elements of matrix \mathbf{E}_l ($K \times 1$) in (23.2) acquire integral form $\frac{1}{2\pi} \int_{-\Omega}^{\Omega} |S(\omega)|^2 e^{j\omega(t-t_l)} d\omega$ or $\frac{1}{2\pi} \int_{-\Omega}^{\Omega} |S(\omega)|^2 e^{j\omega(t-lT)} d\omega$. The inverse transform (23.2) calculated on time moments $t=t_k$ or $t=kT$, $k=0,1,2,\dots,K-1$, returns back the input sequence \mathbf{x} undistorted. Case signal model $S(\omega)=1$ the formulas (22) and (23) reduces to (16) and (17).

The frequency resolution of the EDTFT is in inverse ration to $|S(\omega)|^2 \mathbf{E}_\omega^H \mathbf{R}^{-1} \mathbf{E}_\omega$ and varied in the frequency range $-\Omega \leq \omega \leq \Omega$.

3.3.3 Iterative EDTFT algorithm

Calculation of the EDTFT by formulas (23) requires knowledge of the signal model spectrum which generally is not known. At the same time, the amplitude spectrum obtained in the previous section by the formula (17.3) can be used as a source of such information. This suggests the following iterative algorithm, where the signal model spectrum $S(\omega_0)$ tends to the signal spectrum $S_a(\omega)$:

Iteration 1. Calculate $S_a^{(1)}(\omega)$ (17.3) applying default signal model $S(\omega_0)=1$.

Iteration 2. Calculate $S_a^{(2)}(\omega)$ (23.3) by using the signal model $S_a^{(1)}(\omega_0)$.

Iteration 3. Calculate $S_a^{(3)}(\omega)$ (23.3) by using the signal model $S_a^{(2)}(\omega_0)$.

...

Iteration i. Calculate $S_a^{(i)}(\omega)$ (23.3) by using the signal model $S_a^{(i-1)}(\omega_0)$.

The iterations are repeated until the given maximum iteration number is reached or the power spectrum do not alter from iteration to iteration, $|S_a^{(i)}(\omega)|^2 \approx |S_a^{(i-1)}(\omega)|^2$.

The EDTFT output $F_a(\omega)$ (23.1) is calculated for the last performed iteration I .

By default the signal model $S(\omega_0)=1$ is used as input of the EDTFT algorithm. However, additional information about the signal to be analyzed can be applied to create a more realistic signal model for the EDTFT input and to reduce the number of iterations required to reach the stopping iteration criteria.

4 Extended DFT algorithm

The EDTFT considered in the previous section is a function of continuous frequency ($-\Omega \leq \omega \leq \Omega$), while described below the EDFT algorithm calculate the EDTFT on a discrete frequency set $-\Omega \leq \omega_n < \Omega$ for $n=0,1,2,\dots,N-1$. The number of frequency points $N \geq K$ and it should be selected sufficiently great to substitute the integrals (24) used for calculation of matrix \mathbf{R} ($K \times K$) in the

expressions (22, 23) by the finite sums

$$r_{i,k} = \frac{1}{2\pi} \int_{-\Omega}^{\Omega} |S(\omega_0)|^2 e^{j\omega_0(t_k-t_i)} d\omega_0 \approx \frac{\Omega}{\pi N} \sum_{n=0}^{N-1} |S(\omega_n)|^2 e^{j\omega_n(t_k-t_i)}, \quad (25.1)$$

$$r_{i,k} = \frac{1}{2\pi} \int_{-\Omega}^{\Omega} |S(\omega_0)|^2 e^{j\omega_0(k-l)T} d\omega_0 \approx \frac{\Omega}{\pi N} \sum_{n=0}^{N-1} |S(\omega_n)|^2 e^{j\omega_n(k-l)T}, \quad (25.2)$$

$l, k=0, 1, 2, \dots, K-1$. The matrix composed of (25.1) and (25.2),

$$\mathbf{R} = \begin{bmatrix} r_{0,0}(0) & r_{0,1}(t_1-t_0) & r_{0,2}(t_2-t_0) & \dots & r_{0,K-1}(t_{K-1}-t_0) \\ r_{1,0}(t_0-t_1) & r_{1,1}(0) & r_{1,2}(t_2-t_1) & \dots & r_{1,K-1}(t_{K-1}-t_1) \\ r_{2,0}(t_0-t_2) & r_{2,1}(t_1-t_2) & r_{2,2}(0) & \dots & r_{2,K-1}(t_{K-1}-t_2) \\ \dots & \dots & \dots & \dots & \dots \\ r_{K-1,0}(t_0-t_{K-1}) & r_{K-1,1}(t_1-t_{K-1}) & r_{K-1,2}(t_2-t_{K-1}) & \dots & r_{K-1,K-1}(0) \end{bmatrix}, \quad (26.1)$$

$$\mathbf{R} = \begin{bmatrix} r_{0,0}(0) & r_{0,1}(T) & r_{0,2}(2T) & \dots & r_{0,K-1}((K-1)T) \\ r_{1,0}(-T) & r_{1,1}(0) & r_{1,2}(T) & \dots & r_{1,K-1}((K-2)T) \\ r_{2,0}(-2T) & r_{2,1}(-T) & r_{2,2}(0) & \dots & r_{2,K-1}((K-3)T) \\ \dots & \dots & \dots & \dots & \dots \\ r_{K-1,0}(-(K-1)T) & r_{K-1,1}(-(K-2)T) & r_{K-1,2}(-(K-3)T) & \dots & r_{K-1,K-1}(0) \end{bmatrix}, \quad (26.2)$$

possesses Hermitian symmetry, $r_{i,k} = r_{k,i}^*$, but (26.2) for uniformly sampled signal has also a Toeplitz structure. The matrix elements $r_{i,k}$ representing the autocorrelation function of the selected signal model and can be calculated by applying the IDFT to the signal model power spectrum $|S(\omega_n)|^2$. The frequency $\Omega/\pi=2f_u=f_N$ in (25), where f_u is the signal upper frequency and f_N is the Nyquist rate of a band-limited signal, and it is assumed to be normalized (equal to 1) in DFT calculations. The choice of the frequencies $\{\omega_n\}=\{2\pi f_n\}$ depends on the number of frequencies needed for accurate estimation of (25) as well as for detailed signal spectrum representation, and the limitations on the total amount of computation. Eventually, the uniform set of frequencies is preferable in most application cases.

The EDFT can be expressed by the following iterative algorithm

$$\mathbf{R}^{(i)} = \frac{1}{N} \mathbf{E} \mathbf{W}^{(i)} \mathbf{E}^H, \quad (27.1)$$

$$\mathbf{F}^{(i)} = \mathbf{x} \mathbf{A}^{(i)} = \mathbf{x} (\mathbf{R}^{(i)})^{-1} \mathbf{E} \mathbf{W}^{(i)}, \quad (27.2)$$

$$\mathbf{S}^{(i)} = \frac{\mathbf{x} (\mathbf{R}^{(i)})^{-1} \mathbf{E}}{\text{diag}(\mathbf{E}^H (\mathbf{R}^{(i)})^{-1} \mathbf{E})}, \quad (27.3)$$

$$\mathbf{W}^{(i+1)} = \text{diag}(|\mathbf{S}^{(i)}|^2), \quad (27.4)$$

for the iteration number $i=1, 2, 3, \dots, I$. The exponents matrix \mathbf{E} ($K \times N$) has elements $e^{-j2\pi f_n t_k}$ or $e^{-j2\pi f_n kT}$ if the sampling is uniform. By default the diagonal weight matrix $\mathbf{W}^{(i)}$ ($N \times N$) for the first iteration is a unit matrix $\mathbf{W}^{(1)}=\mathbf{I}$. If other diagonal matrix is used as input of the EDFT algorithm then it must have at least K nonzero elements. For the subsequent iterations $\mathbf{W}^{(i)}$ is filled with power spectrum values calculated by (27.4). There could be additional criteria for stopping the iterations before the maximum number of iterations I is reached, for example, the iterations could be interrupted, if the relative change of the power spectrum $|\text{sum}(\mathbf{W}^{(i)})-\text{sum}(\mathbf{W}^{(i-1)})|/\text{sum}(\mathbf{W}^{(2)})$, for $i>2$, is smaller than a given threshold.

The IDFT can be applied to output \mathbf{F} and return back original K -samples of uniform or nonuniform sequence

$$\mathbf{x} = \frac{1}{N} \mathbf{F} \mathbf{E}^H. \quad (28)$$

Since the length of the frequency set $N \geq K$, then (28) can be modified to obtain a sequence \mathbf{x}_α ($1 \times N$) - $x_\alpha(t_m)$, $m=0,1,2,\dots,N-1$,

$$\mathbf{x}_\alpha = \frac{1}{N} \mathbf{F} \mathbf{E}_N^H, \quad (29)$$

where exponents matrix \mathbf{E}_N ($N \times N$) has elements $e^{-j2\pi f_n t_m}$ or $e^{-j2\pi f_n m T}$ for uniform sampling case. The reconstructed by the formula (29) sequence is the original sequence plus forward and backward extrapolation of \mathbf{x} to length N and/or interpolation if there are gaps inside of \mathbf{x} . The maximum frequency resolution of the iterative algorithm is limited by the length N of frequency set, not by the length K of sequence as in application of classical DFT. This mean, the EDFT is able to increase the frequency resolution N/K times in comparison with the classical DFT. This can be verified by comparing the diagonal elements of the product of IDFT and DFT basis,

$$\text{diag}\left(\frac{1}{N} \mathbf{E}^H \mathbf{E}\right) = K/N < 1, \quad \text{with the relationship,} \quad 0 < \text{diag}\left(\frac{1}{N} \mathbf{E}^H \mathbf{A}\right) = \frac{1}{N} \mathbf{F}./\mathbf{S} \leq 1,$$

corresponding to the IDFT and EDFT basis \mathbf{A} (27.2). At the same time there is a restriction on the frequency resolution $\text{sum}(\mathbf{F}/\mathbf{S})=NK$, which is satisfied by iteration, and in order to achieve a high resolution at certain frequencies, the EDFT must decrease the resolution on other frequencies. The deviation $|\text{sum}(\mathbf{F}/\mathbf{S})-NK|$ also could be used as an additional criteria for stopping of the EDFT iterations, because of indicate the possible inaccuracy in the obtained result, mainly caused by the finite precision in calculations. If this happens, the result of the previous EDFT iteration should be considered as a final one.

In a border-case $N=K$, the iterative algorithm output do not depend on weight matrix \mathbf{W} and the optimal EDFT basis can be found in a non-iterative way (as result of the first EDFT iteration).

5 EDFT and other nonparametric approaches

In the previous sections, starting with the Fourier integral (1) and using its orthogonality property (2), by establishing and solving the minimum least square error estimators (9), the Extended DFT is obtained analytically. Now let's make comparison with other nonparametric methods - Capon filter, Generalized (Weighted) Least Squares (GWLS) solution and High-Resolution Discrete Fourier Transform introduced by Sacchi, Ulrych and Walker in 1998, and try to analyze the ways and opportunities of derivation of an iterative EDFT algorithm based on these approaches.

5.1 Capon filter approach

The Capon filter also known as Minimum Variance spectrum estimate (see [8, 9, 19, 22]) can be viewed as the output of a bank of filters with each filter centered at one of the analysis frequencies

$$y_\omega(nT) = \sum_{k=0}^{K-1} x((n-k)T) h_\omega(kT) = \tilde{\mathbf{x}} \mathbf{h}_\omega, \quad n = 0,1,2,\dots \quad (30)$$

In the matrix notation $\tilde{\mathbf{x}} = [x(nT), x((n-1)T), x((n-2)T), \dots, x((n-K+1)T)]$ is the filter input signal and $\mathbf{h}_\omega = [h_\omega(0), h_\omega(T), h_\omega(2T), \dots, h_\omega((K-1)T)]^T$ is the filter coefficients. Here the subscript ω indicate a dependence on the filter's center frequency.

The Capon filter is designed to minimize the variance on the filter output

$$\sigma_y^2 = \mathcal{E}\{y_\omega(nT)^2\} = \mathcal{E}\{y_\omega^H(nT) y_\omega(nT)\} = \mathcal{E}\{\mathbf{h}_\omega^H \tilde{\mathbf{x}} \tilde{\mathbf{x}}^H \mathbf{h}_\omega\} = \mathbf{h}_\omega^H \mathcal{E}\{\tilde{\mathbf{x}} \tilde{\mathbf{x}}^H\} \mathbf{h}_\omega = \mathbf{h}_\omega^H \mathbf{R}_x \mathbf{h}_\omega, \quad (31)$$

subject to the constraint that its frequency response at the frequency of interest ω has unity gain

$$H(\omega) = \sum_{k=0}^{K-1} h_{\omega}(kT) e^{-j\omega kT} = \mathbf{E}_{\omega}^T \mathbf{h}_{\omega} = 1, \quad (32.1)$$

$$H(\omega) = \sum_{k=0}^{K-1} h_{\omega}^*(kT) e^{j\omega kT} = \mathbf{h}_{\omega}^H \mathbf{E}_{\omega}^* = 1, \quad (32.2)$$

where $\mathcal{E}\{\cdot\}$ denotes the expectation operator and the matrix \mathbf{E}_{ω} ($K \times 1$) has elements $e^{-j\omega kT}$. The constraints (32.1) and (32.2) must be satisfied by the filter (30) and by the Hermitian transpose filter $y_{\omega}^H(nT) = \mathbf{h}_{\omega}^H \tilde{\mathbf{x}}^H$, correspondingly. The matrix $\mathbf{R}_x = \mathcal{E}\{\tilde{\mathbf{x}}^H \tilde{\mathbf{x}}\}$ ($K \times K$) is the sample autocorrelation matrix and it can be composed from the values of the signal autocorrelation function. For example, so called biased estimate is calculated by

$$r_{xx}(lT) = \frac{1}{K} \sum_{k=0}^{K-l-1} x((k+l)T) x^*(kT), \quad l = 0, 1, 2, \dots, K-1 \quad (33)$$

and, taking into account that $r_{xx}(-lT) = r_{xx}^*(lT)$, the sample autocorrelation matrix is filled as

$$\mathbf{R}_x = \begin{bmatrix} r_{0,0}(0) & r_{0,1}(-T) & r_{0,2}(-2T) & \dots & r_{0,K-1}(-(K-1)T) \\ r_{1,0}(T) & r_{1,1}(0) & r_{1,2}(-T) & \dots & r_{1,K-1}(-(K-2)T) \\ r_{2,0}(2T) & r_{2,1}(T) & r_{2,2}(0) & \dots & r_{2,K-1}(-(K-3)T) \\ \dots & \dots & \dots & \dots & \dots \\ r_{K-1,0}((K-1)T) & r_{K-1,1}((K-2)T) & r_{K-1,2}((K-3)T) & \dots & r_{K-1,K-1}(0) \end{bmatrix}. \quad (34)$$

Mathematically, the Capon filter coefficients can be obtained by minimizing the variance (31) under the constrains given by (32.1) and (32.2)

$$J = \mathbf{h}_{\omega}^H \mathbf{R}_x \mathbf{h}_{\omega} - \mu (\mathbf{E}_{\omega}^T \mathbf{h}_{\omega} - 1) - \lambda (\mathbf{h}_{\omega}^H \mathbf{E}_{\omega}^* - 1) = \min, \quad (35)$$

where μ, λ are Lagrange multipliers. The conditions $\frac{\partial J}{\partial \mathbf{h}_{\omega}} = 0$ and $\frac{\partial J}{\partial \mathbf{h}_{\omega}^H} = 0$ have to be fulfilled to determine the minimum of (35). Both requirements lead to the same solution

$$\mathbf{h}_{\omega} = \frac{\mathbf{R}_x^{-1} \mathbf{E}_{\omega}^*}{\mathbf{E}_{\omega}^T \mathbf{R}_x^{-1} \mathbf{E}_{\omega}^*}. \quad (36)$$

and, traditionally, the Capon power spectrum is computed as

$$P_{Capon}(\omega) = \mathbf{h}_{\omega}^H \mathbf{R}_x \mathbf{h}_{\omega} = \frac{1}{\mathbf{E}_{\omega}^T \mathbf{R}_x^{-1} \mathbf{E}_{\omega}^*}. \quad (37)$$

In order to obtain an iterative EDFT algorithm from the original Capon filter approach, the sample autocorrelation matrix \mathbf{R}_x (34) has to be substituted by $\mathbf{R}^T = \mathbf{E}^* \mathbf{W} \mathbf{E}^T$. The matrix \mathbf{R}^T ($K \times K$) can also be obtained as a transpose of the EDFT matrix \mathbf{R} defined by (26). The elements of quadratic diagonal matrix \mathbf{W} ($N \times N$) represent an estimate of power at time moment $nT=0$, determined from one sample at the output of each Capon filter

$$|y_{\omega}(0)|^2 = |\tilde{\mathbf{x}} \mathbf{h}_{\omega}|^2 = \left| \frac{\tilde{\mathbf{x}} (\mathbf{R}^T)^{-1} \mathbf{E}_{\omega}^*}{\mathbf{E}_{\omega}^T (\mathbf{R}^T)^{-1} \mathbf{E}_{\omega}^*} \right|^2, \quad (38)$$

where the filter input sequence $\tilde{\mathbf{x}}$ (30) is related to the EDFT input sequence \mathbf{x} as $\tilde{x}(kT) = x((K+k-1)T)$ or $\tilde{x}(t_k) = x(t_{K+k-1})$, $k=0, -1, -2, \dots, -(K-1)$, for uniformly or nonuniformly sampled sequence cases, respectively.

Finally, an iterative algorithm, with the initial condition for $\mathbf{W}^{(1)} = \mathbf{I}$, can be formed as follows

$$\mathbf{R}^{T(i)} = \mathbf{E}^* \mathbf{W}^{(i)} \mathbf{E}^T, \quad (39.1)$$

$$\mathbf{S}_{Capon}^{(i)} = \frac{\tilde{\mathbf{x}} (\mathbf{R}^{T(i)})^{-1} \mathbf{E}_{\omega}^*}{\text{diag} \left(\mathbf{E}_{\omega}^T (\mathbf{R}^{T(i)})^{-1} \mathbf{E}_{\omega}^* \right)}, \quad (39.2)$$

$$\mathbf{W}^{(i+1)} = \text{diag}(|\mathbf{S}_{\text{Capon}}^{(i)}|^2), \quad (39.3)$$

with the iteration number $i=1,2,3,\dots,I$. The estimate of the power spectrum $|\mathbf{S}_{\text{Capon}}|^2$ coincides with the results of the EDFT, while the phase spectrum, definitely, is different. It should be noted that the calculation of the Capon filter output power by formula (37) is theoretically well justified, whereas the derivation of (39) requires *ad hoc* assumptions and substitutions, and actually is a measurement of power obtained from just a one sample at the output of filter. This leads to conclusion that the approach (39) is simply a filter-bank interpretation of the EDFT, similarly to the DFT which can also be considered as bank of filters. In addition, an iterative algorithm derived on the basis of the filter-bank can not reveal all the EDFT capacity such as the ability to estimate the DFT (27.2) and restore the signal (28, 29).

5.2 GWLS solution

The Generalized (Weighted) Least Squares approach (see [13, 16, 23, 32]) in the frequency analysis is based on the following data model

$$\mathbf{x}^T = \mathbf{E}_\omega^* S_{\text{GWLS}}(\omega) + \mathbf{e}_Q, \quad (40)$$

with \mathbf{e}_Q denoting the noise and interference (signals at frequencies other than ω) component, and $\mathbf{E}_\omega^* S_{\text{GWLS}}(\omega)$ representing the signal component on the frequency of interest with unknown complex amplitude $S_{\text{GWLS}}(\omega)$. The GWLS minimizes

$$[\mathbf{x}^T - \mathbf{E}_\omega^* S_{\text{GWLS}}(\omega)]^H \mathbf{Q}^{-1} [\mathbf{x}^T - \mathbf{E}_\omega^* S_{\text{GWLS}}(\omega)], \quad (41)$$

which is solved by

$$S_{\text{GWLS}}(\omega) = \frac{\mathbf{E}_\omega^T \mathbf{Q}^{-1} \mathbf{x}^T}{\mathbf{E}_\omega^T \mathbf{Q}^{-1} \mathbf{E}_\omega^*}, \quad (42)$$

where \mathbf{Q} ($K \times K$) is the covariance matrix of the data model component \mathbf{e}_Q . There are two special cases of GWLS called Weighted Least Squares (WLS) and ordinary Least Squares (LS). WLS occurs when all the off-diagonal entries of \mathbf{Q} are 0, while LS solution is obtained from the GWLS under assumption that \mathbf{e}_Q in (40) is a white noise, hence $\mathbf{Q}=\mathbf{I}$.

The problem of GWLS estimator is that, in general, the covariance matrix \mathbf{Q} is not known, and must be estimated from the data along with the $S_{\text{GWLS}}(\omega)$. The initial estimate (the 1st iteration) could be equal to LS solution, it is (42) with $\mathbf{Q}=\mathbf{I}$. Next, to ensure that the GWLS solution works in an iterative way as EDFT do, covariance matrix \mathbf{Q} should be replaced by $\mathbf{R}^T = \mathbf{E}^* \mathbf{W} \mathbf{E}^T$. As a result, GWLS solution (42) coincides with the EDTFT formula (23.3)

$$S_{\text{GWLS}}(\omega) = \frac{\mathbf{E}_\omega^T (\mathbf{R}^T)^{-1} \mathbf{x}^T}{\mathbf{E}_\omega^T (\mathbf{R}^T)^{-1} \mathbf{E}_\omega^*} = \frac{\mathbf{x} \mathbf{R}^{-1} \mathbf{E}_\omega}{\mathbf{E}_\omega^H \mathbf{R}^{-1} \mathbf{E}_\omega} = S_\alpha(\omega) \quad (43)$$

and, as shown in the Section 3.3.3, can be successfully used to update the matrix \mathbf{W} and for calculation of the amplitude spectrum iteratively. Although such a substitution would be easy done, it is not supported by GWLS data model (40), from where the matrix \mathbf{Q} represents the data model component \mathbf{e}_Q only and the signal component $\mathbf{E}_\omega^* S_{\text{GWLS}}(\omega)$ must be excluded from it, whereas the matrix \mathbf{R}^T is calculated for the entire signal \mathbf{x}^T , including \mathbf{e}_Q and $\mathbf{E}_\omega^* S_{\text{GWLS}}(\omega)$. Furthermore, the derivation of EDFT shows that the signal can be restored by formula (28), which fits perfectly to the iterative update of the matrix \mathbf{R} . The conclusion reached is that making the derivation of the Extended DFT algorithm possible, invalidates GWLS minimization expression (41) which require separation of both data model components.

5.3 High-Resolution DFT

The third method considered here is the High-Resolution DFT (HRDFT) [7]. The authors

presented an iterative nonparametric approach of spectral estimation, which minimizes the cost function deduced from Bayes' theorem and, as well as the Extended DFT, makes it possible to obtain high-resolution Fourier spectrum. The HRDFT algorithm can be reduced to the following iterative procedure:

$$\mathbf{R}^{(i)} = \frac{1}{N} \mathbf{E} \mathbf{W}^{(i)} \mathbf{E}^H, \quad (44.1)$$

$$\mathbf{F}_{HRDFT}^{(i)} = \mathbf{x}(\mathbf{R}^{(i)})^{-1} \mathbf{E} \mathbf{W}^{(i)}, \quad (44.2)$$

$$\mathbf{W}^{(i+1)} = \text{diag} \left(\frac{1}{N} |\mathbf{F}_{HRDFT}^{(i)}|^2 \right), \quad (44.3)$$

for iteration number $i=1,2,3,\dots,I$ and with the initial condition $\mathbf{W}^{(1)}=\mathbf{I}$.

The IDFT (28) applied for any iteration output (44.2), return back the sequence \mathbf{x} undistorted. The main difference between approaches is that the HRDFT algorithm lack of formula for estimate of amplitude spectrum (27.3). Instead, as input for the next iteration, it uses the Fourier spectrum estimated in previous iteration (44.3). Therefore, the results of the HRDFT differ from output of the EDFT significantly.

6 Computer simulations

The computer modeling of the EDFT algorithm are performed for the complex-value test signal used in [6]. True spectrum of the test signal consisting of a band-limited noise in frequency range $[-0.5\dots-0.25]$ Hz, a rectangular pulse in range $[0\dots0.25]$ Hz and unit power complex exponent at frequency 0.35 Hz. The signal upper frequency is $f_u=0.5$ Hz. Uniform and nonuniform test sequences of length $K=64$ samples are derived by simulating 10-bit Analog-to-Digital Converter (ADC). Sampling and mean sampling periods of both sequences are equal, $T=T_s=1$ s. Sampling time moments for the nonuniform sequence are generated as, $t_k = kT + \tau_k$, $k=0,2,\dots,K-1$, where $\{\tau_k\}$ are uniformly distributed random values in range $[0\dots0.8s]$. Thus, the true spectrum of both test sequences consisting of three non-overlapping components and ADC added floor noise (≈ -60 dB), and it is symbolized by red color lines in the Figures 1-3.

The plots in Figures 1 and 2 shows the performance of EDFT (black line) for uniform and nonuniform sequences and allows to compare it with the classical DFT (blue line). The number of frequencies (the length of DFT) here is chosen to be $N=1000$, which gives spectral estimate with step by frequencies $2f_u/N=0.001$ Hz. The range $[-0.5\dots0.5]$ Hz is uniformly covered by frequencies and used for the calculations of (25, 27) and for the signal representation in the frequency domain (spectrum plots).

Figures 1a and 2a display the power spectrum of the EDFT calculated as $10\lg(|\mathbf{S}|^2)$ in a non-iterative way. The input matrix \mathbf{W} for this case is composed from the values of true spectrum (red line in the plots), therefore there is no need for iterations. The obtained non-iterative EDFT estimate is very close to the EDFT 10th iteration result depicted in Fig.1b and 2b, where the input matrix $\mathbf{W}=\mathbf{I}$ is used for the first iteration. The Figure 1c (2c) shows the Power Spectral Density (PSD) calculated by the EDFT as $10\lg(|\mathbf{F}|^2/N)$ and proves the expectations, that the PSD estimate of complex exponent (0.35 Hz) should increase in a value in comparison with the classical DFT, if the proposed method achieves a high resolution around this frequency.

Figures 1d and 2d plot the relative frequency resolution for the EDFT 10th iteration, calculated as

$\frac{1}{2f_uTK} \mathbf{F}./\mathbf{S}$ case of uniform or $\frac{1}{2f_uT_sK} \mathbf{F}./\mathbf{S}$ case of nonuniform sequence, in respect to the

DFT for which, according to (18.2), it is simply equal to 1 at all frequencies. The value of $2f_uT=2f_uT_s=1$ and this means that the signal is processed in one Nyquist zone. The DFT is showing a normal frequency resolution, whereas the EDFT have ability to increase the resolution

(in plot appears values >1) around the powerful signal components and decrease the resolution (in plot appears values <1) at frequencies where the signal have weak power components. The EDFT is called as high-resolution method and that's true, but with the following remark - it still keeps the same 'summary' resolution as the traditional DFT or, in other words, squares under black and blue curves in the plots 1d (2d) are equal. The maximum frequency resolution is limited by value of division N/K . For example, if $K=64$ and $N=1000$, then the EDFT can

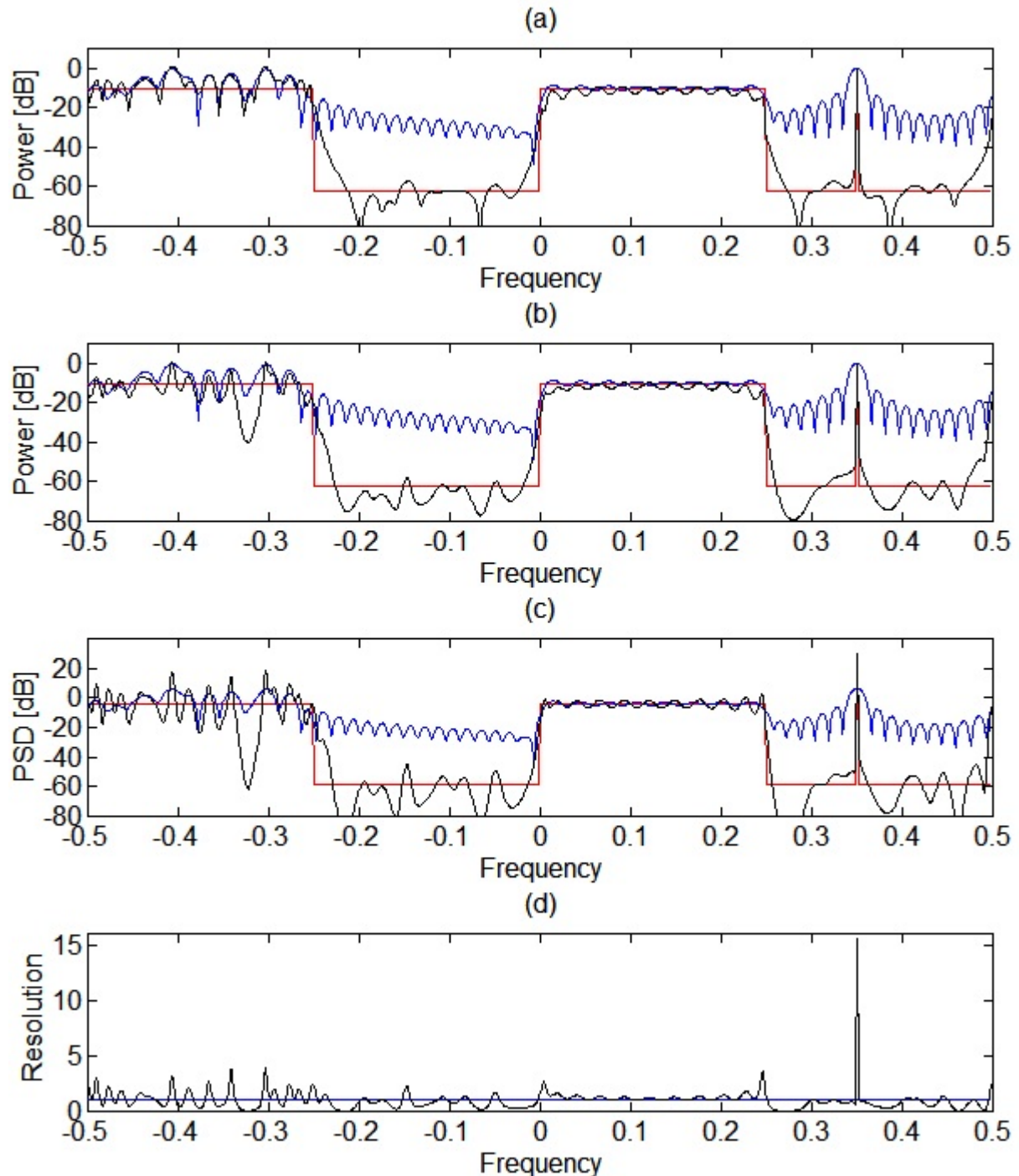


Figure 1. Uniform complex-value test sequence. The estimate of:
 (a) Power spectrum - True (red), DFT (blue) and non-iterative EDFT (black),
 (b) Power spectrum - True (red), DFT (blue) and EDFT (10th iteration),
 (c) Power Spectral Density - True (red), DFT (blue) and EDFT (10th iteration),
 (d) Relative frequency resolution - DFT (blue) and EDFT (10th iteration).

potentially improve the frequency resolution $1000/64 \approx 16$ times. Maximum resolution is achieved on narrow-band signal components, for test signal - at frequency 0.35 Hz. The rectangular pulse is processed by the EDFT with approximately the same resolution as the DFT (≈ 1 , normal frequency resolution), the relative resolution for band-limited noise $[-0.5 \dots -0.25]$ Hz fluctuates around 1, while in the range where just ADC noise can be found, the EDFT decreases the frequency resolution below the normal. The difference between uniform and nonuniform EDFT

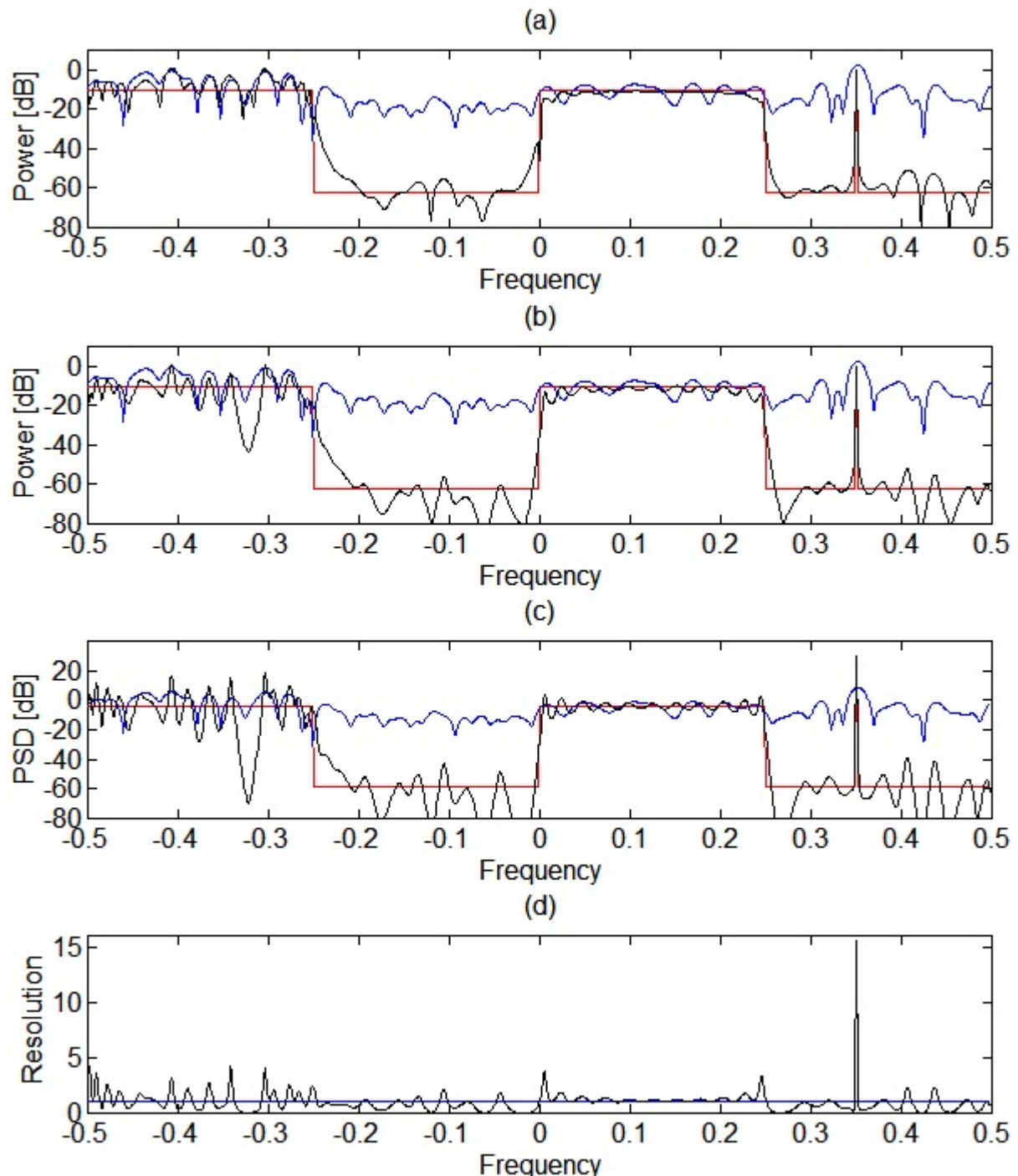


Figure 2. Nonuniform complex-value test sequence. The estimate of:
 (a) Power spectrum - True (red), DFT (blue) and non-iterative EDFT (black),
 (b) Power spectrum - True (red), DFT (blue) and EDFT (10th iteration),
 (c) Power Spectral Density - True (red), DFT (blue) and EDFT (10th iteration),
 (d) Relative frequency resolution - DFT (blue) and EDFT (10th iteration).

is explained in Figure 3, where the same uniform and nonuniform test sequences are analyzed in extended frequency range, $[-1...1]$ Hz. The number of frequency points and the upper frequency are increased two times, $N=2000$ and $f_u=1$ Hz. This means that the step by frequency remains the same as in the previous plots. The true spectrum of test sequences at frequencies above 0.5 Hz consists only of floor noise (≈ -60 dB) added by ADC. The actual result depicted in Figure 3a shows periodicity in the spectrum, which can not be avoided for uniformly sampling sequences. In contrast, the EDFT applied to the nonuniform test sequence gives the correct power spectrum, although this requires more calculations - 15 iterations are performed to obtain an estimate in Figure 3b. The relative frequency resolution of nonuniform EDFT and DFT are compared in Figure 3c. The relative resolution of the nonuniform DFT is calculated as $1/(2f_u T_s)=0.5$ and it is half the normal resolution because of analysis is performed in two Nyquist zones. Nevertheless, the squares under blue and black plots in Figure 3c are equal to one's depicted in Figure 2d. The maximum increase in the frequency resolution $2000/64 \approx 31$ times is achieved on a complex exponent at frequency 0.35 Hz. The EDFT should also increase the resolution in half to process a band-limited noise component ($[-0.5...-0.25]$ Hz) and a pulse ($[0...0.25]$ Hz) with the normal

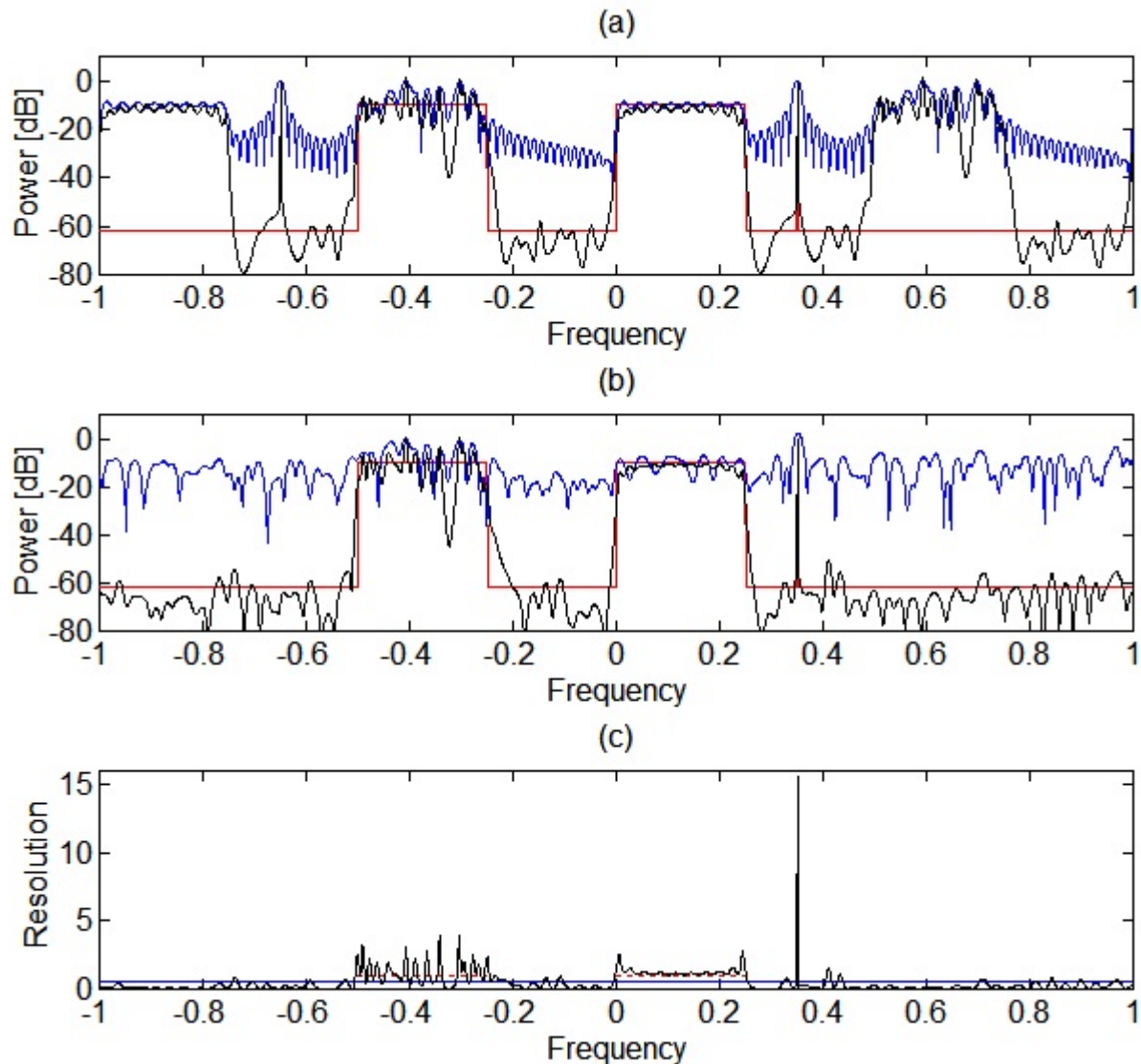


Figure 3. The estimates obtained in the extended frequency range:

- (a) Power spectrum of uniform sequence - True (red), DFT (blue) and EDFT (10th iteration),
- (b) Power spectrum of nonuniform sequence - True (red), DFT (blue) and EDFT (15th iteration),
- (c) Relative frequency resolution of nonuniform sequence- DFT (blue) and EDFT (15th iteration).

frequency resolution equal to 1, as it is indicated by the red dotted lines in Figure 3c. Hence the conclusion that EDFT can handle nonuniformly sampled signals in multiple Nyquist zones, but the spectrum of the signal components if its sum, still must not exceed a one Nyquist zone. Let's check fulfilling of this condition on a test sequence. Since spectrum of the uniform sequence (see the red color lines in Figure 1) covers more than half of Nyquist zone, EDFT should be able to handle it with mean sampling period $T_s < 2T$. The increase of T_s will be achieved by skipping of samples from the original sequence randomly. The result can be considered as nonuniformly sampled sequences as the distance between adjacent readings becomes unequal [5]. The power spectrum depicted in Figure 4 shows the impact of sample skipping on the performance of DFT and EDFT. The inputs are modeled by removing 16, 24 and 32 samples randomly from the uniform 64-point test sequence, and leads in increase of mean sampling period T_s , $64/48T=1,33s$, $64/40T=1,6s$ and $64/32T=2s$, correspondingly. The length of DFT is kept $N=1000$ and frequencies are uniformly spread in the range $[-0.5...0.5]$ Hz. The simulations showing that DFT is not able to handle sequences with missed samples, while EDFT is still applicable if one Nyquist zone condition for the signal is satisfied (Figure 4a and 4b), otherwise the results becomes worse (Figure 4c). Also processing of time localized pulse requires the denser sampling. That's why a rectangular pulse in range $[0...0.25]$ Hz not recovered by the EDFT in Figure 4b.

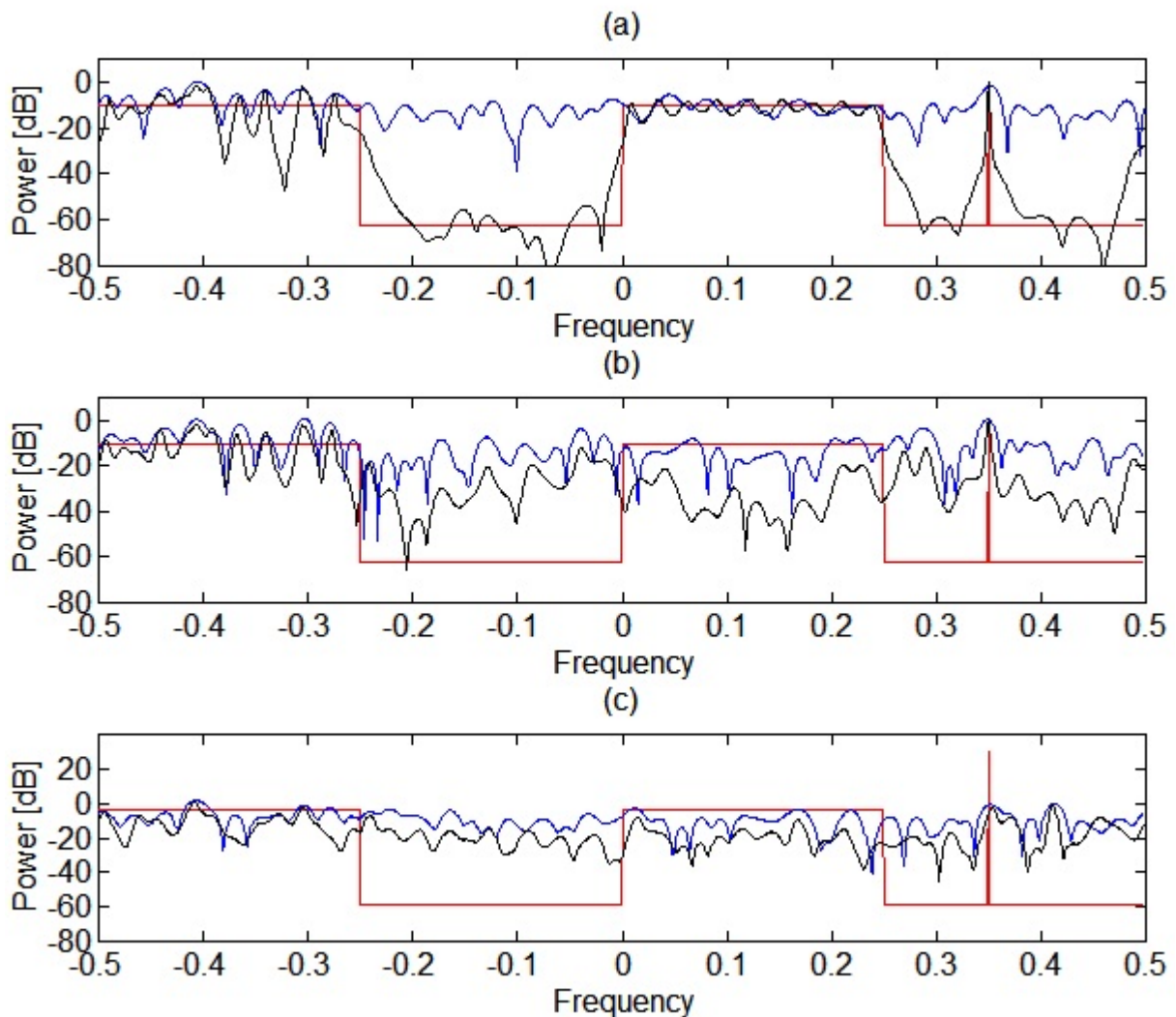


Figure 4. The power spectrum - True (red), DFT (blue) and EDFT (10th iteration), of test sequence with randomly skipped 16 (a), 24 (b) and 32 (c) samples.

The third test sequence used in computer simulations is well-known Marple&Kay data set taken from [1]. It is 64-point real sample sequence from a process consisting of two unit power harmonics with frequencies of 0.2 and 0.21 Hz, a third harmonic with a power of 0.1 (20 dB down) at 0.1 Hz and a colored noise in frequency range [0.2...0.5] Hz (see red color lines in Figure 5). The signal upper frequency is $f_u=0.5$ Hz and the length of DFT is selected $N=1000$. Only 500 positive frequencies are shown, because of the Marple&Kay sequence is real-valued and negative frequencies, if depicted, gives a symmetrical pattern to zero frequency. The Figure 5 shows the power spectrum of the DFT, EDFT and HRDFT approaches in a common view, while separately these plots have been presented in [3] and [7]. The performance of other well-known spectral analysis methods for Marple&Kay data set can be found in [1], including Minimum Variance approach, named in the Section 5.1 as traditional Capon filter (37).

The simulation results in the Figure 5a,b demonstrate, that the classical DFT and EDFT able to evaluate not only the spectrum of sinusoids, but also the shape of continuous spectrum of other signal components, whereas HRDFT on Figure 5c is suitable mostly for the estimation of line spectrum. The plot in Figure 5a showing that due to limited frequency resolution the classical DFT cannot resolve sinusoids at frequencies 0.2 and 0.21. Although the first EDFT iteration coincides with the DFT, in subsequent iterations the EDFT is able to increase the frequency

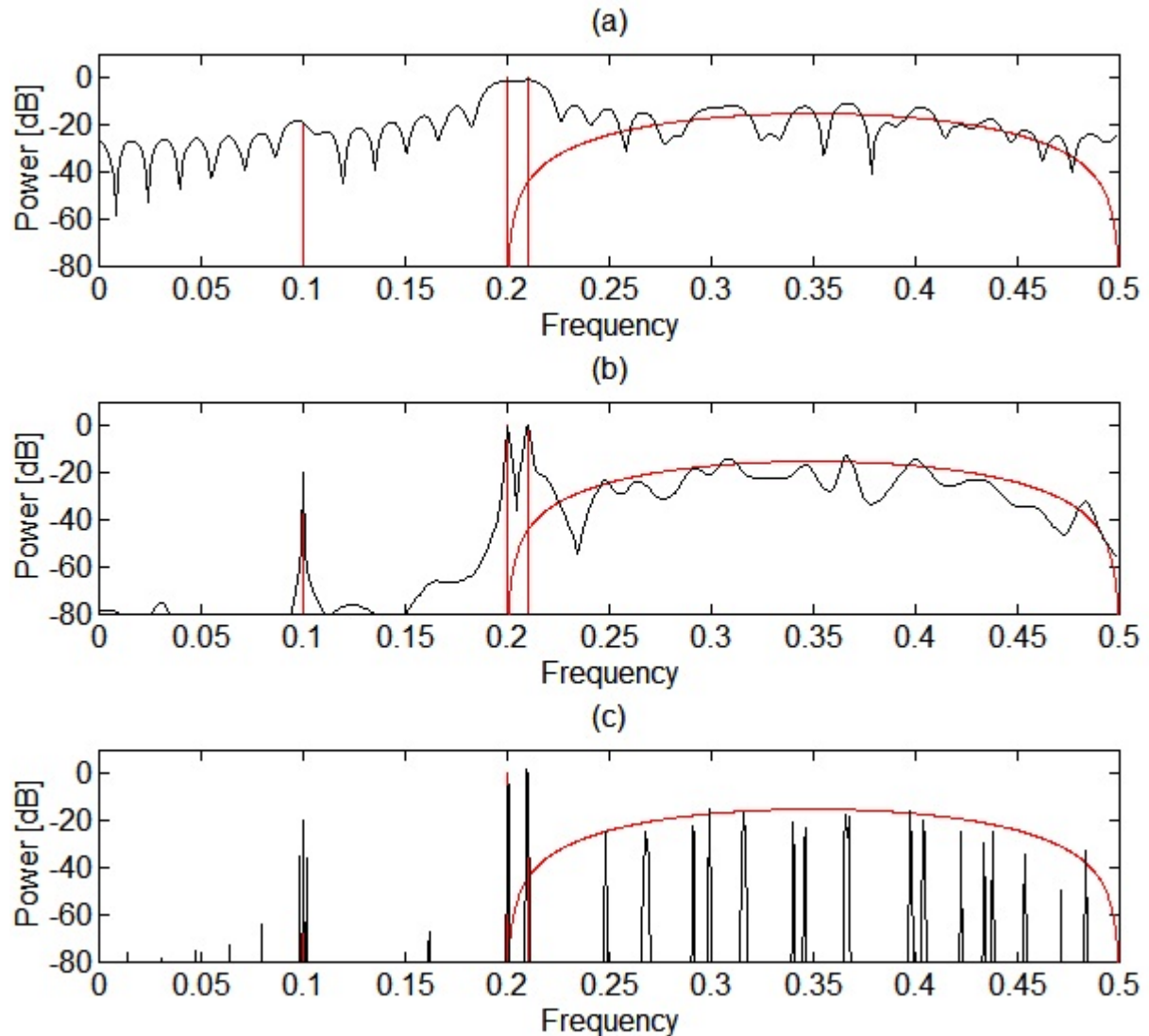


Figure 5. The power spectrum obtained for Marple&Kay data set by (a) DFT, (b) EDFT (10th iteration), (c) HRDFT (10th iteration).

coincides with the DFT, in subsequent iterations the EDFT is able to increase the frequency resolution around the powerful signal components and all three sinusoids are clearly distinguished after 10 iterations in Figure 5b.

All the three DFT have one common feature - the ability to get back 64 samples of Marple&Kay data set by applying the IDFT to the output of each of these methods. Since the length of the DFT is chosen equal to 1000, the inverse transform returns 1000-64 additional samples, which are plotted in Figure 6 in the black. The samples 65, 66, 67,... are considered as a forward extrapolation, but samples 1000, 999, 998,... as a backward extrapolation of known 64-sample sequence (blue). Of course, the Marple&Kay sequence outside of given data set is unknown, and plots on Figure 6 are just a three possible versions of its extrapolation. The classical DFT (Fig.6a) suggests that Marple&Kay sequence outside of given 64 samples will be zeros, the HRDFT (Fig.6c) shows that the extrapolated data even will increase in power, while the EDFT (Fig.6b) expects that the sequence beyond will have approximately the same power, which only gradually decreases with time.

Any approach, that claims that it is a high frequency resolution method, in accordance with the Uncertainty Principle must make certain assumptions about the data outside of the observation period, even if by itself it is not able to recover the signal. The advantage of the proposed method

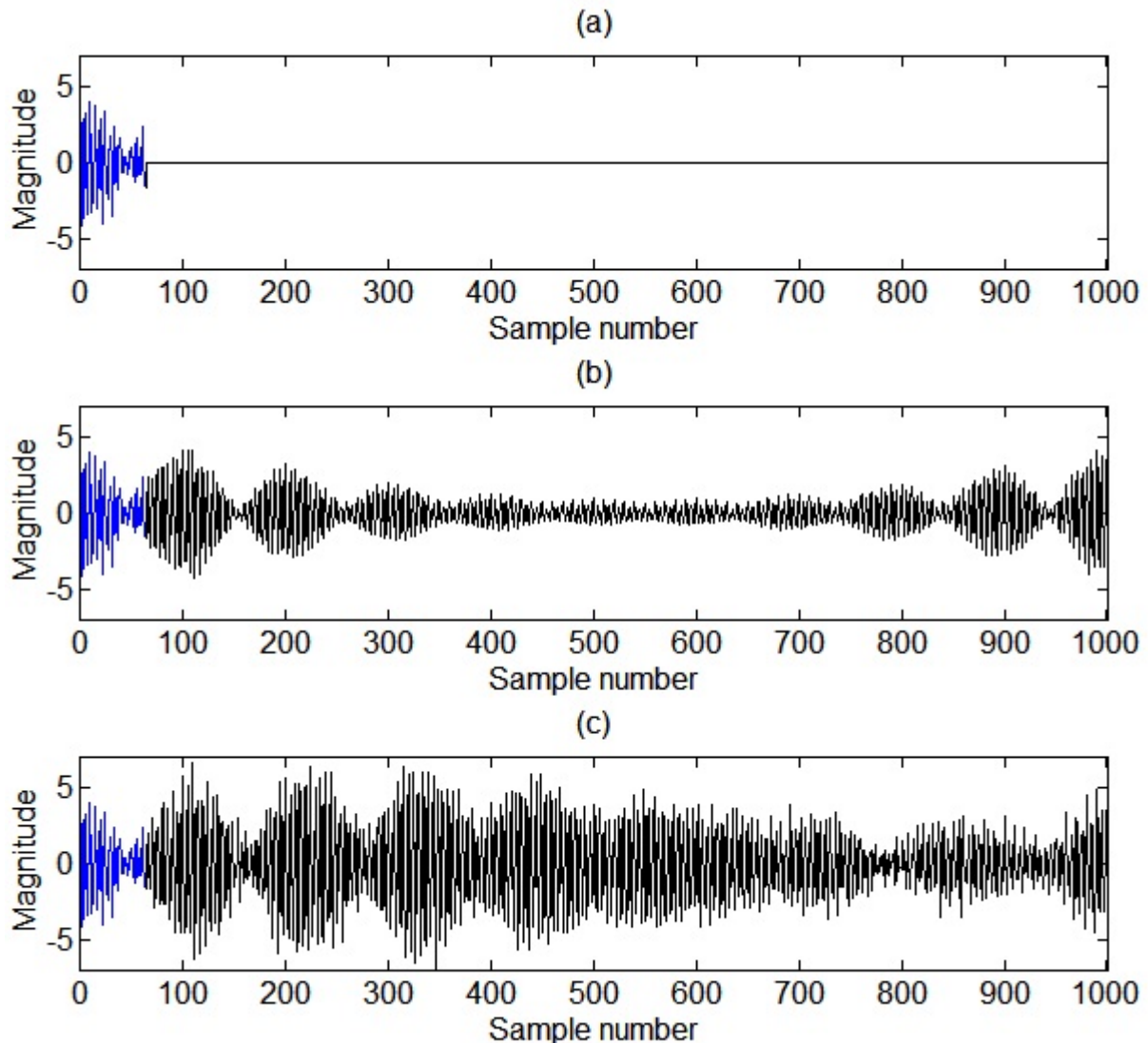


Figure 6. True Marple&Kay real-value sequence (blue) and extrapolated data (black) by (a) DFT, (b) EDFT (10th iteration), (c) HRDFT (10th iteration).

over similar ones is that EDFT based on a solution that satisfies the minimum least squares criteria (6), making it an accurate, reliable and stable.

Run MATLAB program EDFT_FIG.m available on file exchange (see link below) to recreate the computer simulation results presented in this section.

7 EDFT algorithm in MATLAB code

The package consisting of MATLAB programs: NEDFT.m and INEDFT.m, EDFT.m and EDFT2.m, is created to demonstrate the Extended DFT capabilities described in the previous sections. The program NEDFT.m and the inverse transform INEDFT.m can be run for nonuniformly or uniformly sampled signals and for arbitrary selected frequency sets. From the calculations complexity viewpoint, it is reasonable to select the frequencies on the same grid as used by the Fast Fourier Transform algorithm (FFT.m in MATLAB code). The program EDFT.m is designed as a faster realization of the proposed method, where the algorithm described in [5] is implemented. This program is applicable for uniformly sampled signals and for signals with missing samples or data segments (gaps) inside of the input sequence. The inverse transform to EDFT.m is MATLAB program IFFT.m. The EDFT2.m and its inverse IFFT2.m can be used in 2-dimensional signal processing. See the programs help for more details.

The first version of EDFT (file GDFT.m) was submitted on 10/7/1997 as MATLAB 4.1 code. The renewed code version uploaded on 8/5/2006 and available online <http://www.mathworks.com/matlabcentral/fileexchange/11020-extended-dft>.

Please note that programs have not been tested on the latest MATLAB versions and therefore have opportunities to performance improvements (see for example [23, 26]).

8 References

- [1] S.M. Kay, S.L. Marple. Spectrum analysis - a modern perspective. Proc. IEEE, Vol.69, No.11, 1981.
- [2] V. Liepin'sh. A method for spectral analysis of band-limited signals, Automatic Control and Computer Sciences. Vol.27, No.5, pp. 56-63, 1993.
- [3] V. Liepin'sh. A method for spectrum evaluation applicable to analysis of periodically and non-regularly digitized signals. Automatic Control and Computer Sciences, Vol.27, No.6, pp. 57-64, 1993.
- [4] V. Liepin'sh. A spectral estimation method of nonuniformly sampled band-limited signals. Automatic Control and Computer Sciences, Vol.28, No.2, pp. 66-73, 1994.
- [5] V. Liepin'sh. An algorithm for evaluation a discrete Fourier transform for incomplete data. Automatic Control and Computer Sciences, Vol.30, No.3, pp.27-40, 1996.
- [6] Vilnis Liepins. High-resolution spectral analysis by using basis function adaptation approach. Doctoral Thesis for Scientific Degree of Dr. Sc. Comp. */in Latvian/*, University of Latvia, 1997. Abstract available on <http://hdl.handle.net/10068/330816>.
- [7] M.D. Sacchi, T.J. Ulrych, C. Walker. Interpolation and extrapolation using a high-resolution discrete Fourier transform. IEEE Trans. on Signal Processing, Vol.46, No.1, pp. 31-38, 1998.
- [8] Modris Greitans. Multiband signal processing by using nonuniform sampling and iterative updating of autocorrelation matrix. Proceedings of the 2001 International Conference on Sampling Theory and Application, May 13-17, 2001, Orlando, Florida, USA, pp. 85-89.
- [9] Modris Greitans. Spectral analysis based on signal dependent transformation. The 2005 International Workshop on Spectral Methods and Multirate Signal Processing, (SMMSPP 2005), June 20-22, 2005, Riga, Latvia.

- [10] Jayme Garcia Arnal Barbedo, Amauri Lopes, Patrick J. Wolfe. High Time-Resolution Estimation of Multiple Fundamental Frequencies. Proceedings of the 8th International Conference on Music Information Retrieval, ISMIR 2007, Sept. 23-27, Vienna, Austria, pp. 399-402.
- [11] David Dolenc, Barbara Romanowicz, Paul McGill, William Wilcock. Observations of infragravity waves at the ocean-bottom broadband seismic stations Endeavour (KEBB) and Explorer (KXBB). *Geochemistry, Geophysics, Geosystems*, Vol.9, Issue 5, May 2008.
- [12] Quanming Zhang, Huijin Liu, Hongkun Chen, Qiongli Li, Zhenhuan Zhang. A Precise and Adaptive Algorithm for Interharmonics Measurement Based on Iterative DFT. *IEEE Trans on Power Delivery*, Vol.23, Issue 4, pp. 1728-1735, Oct. 2008.
- [13] Petre Stoica, Jian Li, Hao He. Spectral Analysis of nonuniformly Sampled Data: A New Approach Versus the Periodogram. *IEEE Trans on Signal Processing*, Vol.57, Issue 3, pp. 843-858, March 2009.
- [14] Eric Greenwood, Fredric H. Schmitz. Separation of Main and Tail Rotor Noise Sources from Ground-Based Acoustic Measurements Using Time-Domain De-Dopplerization. 35th European Rotorcraft Forum 2009, Sept. 22-25, Hamburg, Germany.
- [15] Jayme Garcia Arnal Barbedo, Amauri Lopes, Patrick J. Wolfe. Empirical Methods to Determine the Number of Sources in Single-Channel Musical Signals. *IEEE Transactions on Audio, Speech and Language Processing*, Vol.17, Issue 7, pp. 1435-1444, Sept. 2009.
- [16] Tarik Yardibi, Jean Li, Petre Stoica, Ming Xue, Arthur B. Baggeroer. Source localization and sensing: A nonparametric iterative adaptive approach based on weighted least squares. *IEEE Transactions on Aerospace and Electronic Systems*, Vol.46, pp. 425-443, Jan. 2010.
- [17] M. Caciotta, S. Giarnetti, F. Leccese, Z. Leonowicz. Comparison between DFT, adaptive window DFT and EDFT for power quality frequency spectrum analysis. *Modern Electric Power Systems (MEPS)*, 2010 Proceedings of the International Symposium, Sept. 20-22, 2010, Wroclaw, pp. 1-5.
- [18] Li Li, Yan Zheng, Wang Xing-zhi. Inter-harmonic Analysis Using IGG and Extended Fourier. *Proceedings of the Chinese Society of Universities for Electric Power System and its Automation*, 22(3), 2010.
- [19] Erik Gudmundson, Andreas Jakobsson, Jörgen Jensen, Peter Stoica. An Iterative Adaptive Approach for Blood Velocity Estimation Using Ultrasound. 18th European Signal Processing Conference (EUSIPCO), Aalborg, Denmark, Aug 23-27, 2010, pp. 348-352.
- [20] Modris Greitans, Rolands Shavelis. Reconstruction of sequences of arbitrary shaped pulses from its low pass or band pass approximations using spectrum extrapolation. *EUSIPCO 2010*, Aug. 23-27, Aalborg, Denmark, pp. 1607-1611.
- [21] Juggrapong Tretrong. Fault Detection of Electric Motors Based on Frequency and Time-Frequency Analysis using Extended DFT. *International Journal of Control and Automation*, Vol.4 No.1, March 2011.
- [22] Jesper Rindom Jensen, Mads Græsbøll Christensen, Søren Holdt Jensen. A Single Snapshot Optimal Filtering Method for Fundamental Frequency Estimation. 36th International Conference on Acoustics, Speech and Signal Processing (ICASSP), Prague, Czech Republic, May 22-27, 2011, pp. 4272-4275.
- [23] Ming Xue, Luzhou Xu, Jian Li. IAA spectral estimation: fast implementation using the Gohberg-Semencul factorization. *ICASSP2011*, May 22-27, Prague, Czech Republic, pp. 3251-3261.
- [24] Bonifatius Wilhelmus Tilma. Supervisor: M.K. Smit; Co-promotor: E.A.J.M. Bente. Integrated tunable quantum-dot laser for optical coherence tomography in the 1.7 μ m wavelength region. Eindhoven, Technische Universiteit Eindhoven, Diss., Jun. 2011.

- [25] Elmar Mair, Michael Fleps, Michael Suppa, and Darius Burschka. Spatio-temporal initialization for IMU to camera registration. In Proceedings of the IEEE International Conference on Robotics and Biomimetics (ROBIO), Dec. 2011, pp. 557-564.
- [26] George-Othan Glentis, Andreas Jakobsson. Superfast Approximative Implementation of the IAA Spectral Estimate. IEEE Transactions on Signal Processing, Vol.60, Issue 1, Jan. 2012, pp. 472-478.
- [27] B. W. Tilma, Yuqing Jiao, J. Kotani, B. Smalbrugge, H. P. M. M. Ambrosius, P. J. Thijs, X. J. M. Leijtens, R. Notzel, M. K. Smit, E. A. J. M. Bente. Integrated Tunable Quantum-Dot Laser for Optical Coherence Tomography in the 1.7 μm Wavelength Region. IEEE Journal of Quantum Electronics, Vol.48, No.2, Feb. 2012, pp. 87-98.
- [28] T. Odstrcil, M. Odstrcil, O. Grover¹, V. Svoboda¹, I. Ďuran¹, and J. Mlynář. Low cost alternative of high speed visible light camera for tokamak experiments. Review of Scientific Instruments. Oct. 2012, Vol.83, Issue 10.
- [29] Elmar Mair. Co-promotor: Gregory Donald Hager. Efficient and Robust Pose Estimation Based on Inertial and Visual Sensing. München, Technische Universität München, Diss., 2012.
- [30] Akash K Singh. Quantum-Dot Laser OCT. International Journal of Engineering Research and Applications (IJERA), Vol.2, Issue 6, Nov.- Dec. 2012, pp.340-371.
- [31] Elliot Briggs, OFDM Physical Layer Architecture and Real-Time Multi-Path Fading Channel Emulation for the 3GPP Long Term Evolution Downlink. PhD Thesis. Texas Tech University, Dec. 2012.
- [32] Kwadwo S. Agyepong, Fang-Han Hsu, Edward R. Dougherty and Erchin Serpedin. Spectral Analysis on Time-Course Expression Data: Detecting Periodic Genes Using a Real-Valued Iterative Adaptive Approach. Advances in Bioinformatics, Vol. 2013.